coatings

MDPI

Article

Assessing of the Road Pavement Roughness by Means of LiDAR Technology

Maria Rosaria De Blasiis [1,*], Alessandro Di Benedetto [2], Margherita Fiani [2] and Marco Garozzo [3]

[1] Department of Engineering, University of Roma TRE, 00146 Rome, Italy
[2] Department of Civil Engineering, University of Salerno, 84084 Fisciano, Italy; adibenedetto@unisa.it (A.D.B.); m.fiani@unisa.it (M.F.)
[3] Sina Spa, 20135 Milano, Italy; marco.garozzo@sina.co.it
* Correspondence: mariarosaria.deblasiis@uniroma3.it; Tel.: +39-657333443

Abstract: The assessment of the road roughness conditions plays an important role to ensure the required performances related to road safety and ride comfort, furthermore providing a tool for pavement maintenance and rehabilitation planning. In this work, the authors compared the roughness index (International Roughness Index, IRI) derived from high speed inertial profilometer with two other roughness indices, one dynamic and one geometric computed on a digital elevation model (DEM) built by using mobile laser scanner (MLS) data. The MLS data were acquired on an extra-urban road section and interpolated on the nodes of a DEM with a curvilinear abscissa, coinciding with the global navigation satellite system (GNSS) track of the profilometer. To estimate the grid cell elevation, we applied two interpolation methods, ordinary kriging (OK) and inverse distance weighting (IDW), over the same data. The roughness values computed on the surface of the DEM showed a similar trend and a high correlation with those acquired by the profilometer, higher for the dynamic index than for the geometric index. The differences between the IRI values by profilometer and those computed on the DEM were small enough not to significantly affect the judgments on the analyzed sections. Moreover, the road sub-sections derived from profilometer measure that were classified as critical coincided with those derived from light detection and ranging (LiDAR) surveys. The proposed method can be used to perform a network-level analysis. In addition, to evaluate the effects of vibrations on human comfort, we input the DEMs into a dynamic simulation software in order to compute the vertical accelerations, as specified in the UNI ISO 2631 standard. The values obtained were in line and correlated with those inferred from the standard methodology for profilometer measures.

Keywords: MLS; DEM; profilometer; IRI; pavement management; ride comfort

check for updates

Citation: De Blasiis, M.R.; Di Benedetto, A.; Fiani, M.; Garozzo, M. Assessing of the Road Pavement Roughness by Means of LiDAR Technology. *Coatings* **2021**, *11*, 17. https://dx.doi.org/10.3390/coatings11010017

Received: 3 December 2020
Accepted: 23 December 2020
Published: 25 December 2020

Publisher's Note: MDPI stays neutral with regard to jurisdictional claims in published maps and institutional affiliations.

Copyright: © 2020 by the authors. Licensee MDPI, Basel, Switzerland. This article is an open access article distributed under the terms and conditions of the Creative Commons Attribution (CC BY) license (https://creativecommons.org/licenses/by/4.0/).

1. Introduction

Roughness is a major parameter for the pavement surface. It depends on surface irregularities and therefore affects drive quality and road safety [1]. Road maintenance is usually based on the assessment of roughness [2], as well as on vehicle delay costs and fuel consumption.

The regularity of the pavement affects vehicle vibration (produces accelerations that can be felt by the driver of the vehicle, consequently reducing ride comfort), driving speed, and tire wear. The conditions of a road pavement are defined by specific or global performance indices, which summarize its regularity by numerical values and evaluation scales. In particular, they can be geometric or dynamic and are computed along the longitudinal and transverse surface profiles of the road surface, while others are based on the punctual measurement of the various degradations.

The International Organization for Standardization ISO 13473-2:2002 [3] defines surface regularity as the deviation of the road surface from a true planar surface, and in part 3 (ISO 13473-3:2002 [4]), requirements for profilometer are specified. The American Society

for Testing and Materials (ASTM) associates regularity with the effects it has on vehicle dynamics (ASTM E867-06) [5].

In 1986, the World Bank [6] introduced the International Roughness Index (IRI), which is the most common parameter cited in the literature to provide an objective measure of roughness, with the aim of solving the main issue of the reproducibility and stability of the measurement over time of longitudinal regularity. The IRI is computed as the ratio between the cumulative displacement and the given distance travelled [7].

The computational method is based on the dynamic response of a mathematical model called "quarter-car". The obtained measure is called ARS (average rectified slope) and is obtained from a reference instrument RARS (reference ARS). Because the dynamic response of the model depends on the speed, in the IRI, a reference speed of 80 km/h is defined for practical and technical reasons. The IRI is therefore the RARS obtained at 80 km/h (RARS80). The RARS index matches with the choice made in the National Cooperative Highway Research Program (NCHRP) Report 228 [8] as a calibration method for IRI measures. The index strictly refers to a reference RTRRMS (response-type road roughness measuring systems), has a good accuracy, and is compatible with other profilometric measures.

Currently, three types of profilometers exist: static, low-speed, and high-speed. Static profilometers and rod and level are considered the reference and the most accurate instruments [7]. They are used to calibrate all other equipment [9]. For the comparison of measurements made with different techniques, the standard UNI EN 13036-5:2019 [10] provides guidelines for the evaluation of the irregularities through the digitized longitudinal profile.

The standardized static methods, rod and level (ASTM E 1364-95 [11]) and straight edge (UNI EN 13036-7 [12]), are based on geometric surface analysis.

A number of studies on the correlation between geometric and dynamic indices have shown that the significance of geometric indices is not lower than that of dynamic indices [13–15].

High-speed profilometers, versus low-speed and static, are more efficient; tests can be run under traffic and the operational environment is safer for operators. However, they suffer from several drawbacks, one of which is the reliability of the survey at a speed of 80 km/h and at constant speed [16]. In order to avoid measurement errors in the presence of speed limits or strong variations in vehicle speed, it is necessary to adjust the settings of the quarter car model or to introduce new indicators [17].

Another critical issue of such profilometers is to verify accuracy and repeatability of the measurement by comparing it with the "true roughness", which can be derived by calibrating the profilometer with low-speed or static profilometers and filtering the data for the effects of the vertical displacement of the vehicle [18].

Among the class 1 profilometers, which are those that provide higher accuracy IRI values [19], are the lightweight inertial profilers and manually operated devices (dipstick, walking profiler) [20]. Among the limitations of high-speed measurements, we can include the choice of the profile data intervals with respect to the choice of the filtering technique both for the comparison with other profilometers and to evaluate the effect of the length of the profile data intervals with respect to the length of the surveyed section.

According to Sayers [6], the non-critical components of the wavelength are those outside the 1.52 to 30.5 m range. The IRI computational algorithm filters out those components, and hence IRI values should not be interpreted for wavelengths shorter than 30.5 m.

In the USA or Canada, IRI report interval 7.62 or 10 m allows for the detection of localized roughness and isolated defects that lead to peak values [20]. These peaks on longer sections would be averaged and therefore irregularities would not be detected, and therein an anti-aliasing filter can be applied to reduce this effect [7].

The repeatability of the survey is another critical factor for high-speed profilometers, related to the number of lasers placed on the profilometer bar. The most commonly used profilometers in the world (with the exception of Slovakia equipped with 13 lasers) are equipped with one or two lasers located at the extremities of the profilometer bar [20].

Such configuration, besides producing a partial survey of the road surface, provides a result that is strongly influenced by the trajectory.

Sayers and Karamihas [21] proved how a little variation in the vehicle's trajectory can produce a high variation (20%) on the IRI value computed in a 300 m long road segment. Another major issue is not being able to determine univocally the "start location and lateral position" [9], a prerequisite to ensure the repeatability of the measurement.

Transport agencies in recent years needed to produce better results/profits using fewer and fewer resources. One way they can increase productivity is through the use of new technologies. These include LiDAR (light detection and ranging) technology, which is currently one of the most interesting remote sensing techniques for infrastructure applications [22–25]. Laser scanners (LS), which are based on this technology, provide very accurate and high-resolution 3D data through dense point clouds.

Recent advances in sensor electronics and data processing make these technologies worth using. Assessments of the accuracy of an LS survey carried out on roads showed that this 3D data output is well suited for the analysis of both the regularity and geometry of roads where high accuracy in surveying is required [26].

The LS technique makes it possible to determine a "true" profile more effectively than traditional static methods. It also offers a further advantage because it provides data on the whole road surface and therefore gives the possibility to characterize the regularity of the road along the whole carriageway, instead of only along some trajectories [27–29]. A test showed that the spectral density of the profiles derived from LS is in line with that derived from the main traditional techniques; this highlights the reliability of the technique since it shows the same wavelength sensitivity obtained with the standard methods [27].

Profilometer measurements performed using multi-laser profilometers combined with high precision level have a 99% correlation with the data acquired by static LS [30]. A very useful device is the mobile laser scanner (MLS), a laser scanning system that allows for the acquisition of 3D data by means of one or more laser scanners mounted on a mobile platform [31].

MLS systems are significantly more efficient than static systems, terrestrial laser scanner (TLS). A freeway section about 80 km long can be surveyed in 3 h using an MLS, whereas using a TLS, the time required can exceed 120 working days [32]. Mobile LiDAR, a technology widely used since the end of the 20st century, when the first mobile LiDAR system became commercially available [33], has gained attention on applications mainly related to transports [34].

The point cloud obtained from MLS makes it possible a complete inventory of all the elements that make up the infrastructure, from the characterization of road geometry to that of signage and artwork [31]. Safety, efficiency, and cost benefits from MLS technology are highlighted [35].

Mendenhall [36] analyzed the efficiency of the MLS technique in terms of cost and acquisition time. The study was conducted on a 15-mile stretch of an urban street in the city of San Francisco; compared to standardized techniques, the cost savings was estimated to be between USD 200,000 and 300,000, with the time of acquisition reduced by 6 to 8 weeks, further reducing the management time by 4 weeks. The measurement was carried out by a team of operators on a vehicle equipped with MLS travelling on the road at operating speed. MLS scans repeated over time helped the initial design, estimation of the percentage of completion, project compliance, and as-built project drawings, significantly reducing costs and acquisition time compared to traditional methods [37].

There are many reasons that lead the authors to propose LiDAR technology as a support/alternative to the profilometer technique for the measurement of road surface roughness; for example, unlike most profilometers, LiDAR technology does not need to be limited in speed range for correct operating (for profilometers usually from 20 to 100 km/h). Some profilometers are not able to measure on very badly damaged roads or stone and dirt roads, and they are also very sensitive to humidity/temperature of the pavement.

Another key aspect is that, in most cases, the equipped vehicle is able to measure the whole surface in one-way pass; these data are georeferenced with respect to an external reference system, allowing the repeatability of the measurement and allowing the unambiguous positioning of the points belonging to the surface to be compared with measurements made later for the study of the damaging trend.

In more recent times, several applications in the road field have been carried out to validate the use of LiDAR technology. Alhasan [38] acquired point clouds by TLS on different types of concrete Portland cement (PCC) and asphalt concrete (AC) pavements for the assessment of road roughness on unpaved roads; correlations with California bearing ratio (CBR) and dynamic cone penetration (DCP) have also been performed.

Alhasan [39] used the laser technique to evaluate roughness using a variety of methodologies: IRI, fast Fourier transform (FFT), and statistical analysis for the measurement of heights.

Kumar et al. [40] proposed an algorithm that allows users to assess roughness from a point cloud acquired through MLS. The aim of the authors was to identify a methodology able to provide fast, inexpensive, and complete information about regularity by determining the standard deviation of elevation values with respect to an interpolated planar surface.

A fast and automatic identification of localized surface defects is possible even using only the intensity of the reflected beam; morphological functions and special filters allow their identification [41].

Tran and Taweep [42] developed a segmentation algorithm, based on point cloud voxelization, able to estimate the roughness of road surfaces. The method has given excellent results, demonstrating the validity of operating with geometric methods. In addition, a few studies have been performed on potential improvements in inertial profilometers, adding new sensors recently made available such as non-contact wide-footprint and multi-point height sensors [43,44].

Over the years, interdisciplinarity has been a key factor for research, given the complexity of the various phenomena that occur in the characterization of the road/vehicle/user interaction. Liu and Herman [45] introduced a theoretical and detailed description of the vehicle–road interaction together with the analysis of the drive comfort. By using the quarter-car model and applying spectral density analysis, they studied the analytical expressions of dynamic indices, including the acceleration rate (jerk), the rectified mean speed (ARV), the ARS, and the IRI index. One year later, the same authors pointed out that the jerk index is one of the most important parameters for assessing the accessibility and regularity of roads in terms of comfort [46].

A few studies have recently been published to add to the computation of the IRI on the basis of riding comfort. Fuentes et al. [47] analyzed the subjective perception of the user about the level of comfort of a road pavement and the vertical accelerations through the analysis of deterministic and probabilistic models for the estimation of the pavement maintenance, specific for urban roads at low operating speed. Zhang et al. [48] introduced new IRI threshold values on the basis of riding comfort; three different evaluation techniques were used: a questionnaire, a vibration acceleration method, and a psychological and physiological index root mean square of the successive differences (RMSSD) method.

It is then easy to understand how there is already a need to introduce more complex methodologies that are able to simulate the dynamic response of a vehicle as faithfully as possible in order to evaluate its effects. The limitations were mainly due to measurement techniques that did not make it possible to address the problem in its real complexity.

The possibility of obtaining 3D data of the road surface on which to simulate "full car" models has only recently been applied [49] due to the rapid development and reliability of commercial dynamic simulation software. Studies have confirmed the good correspondence between the dynamic responses obtained from simulation and those measured by the instrumented vehicle. There are different studies on this subject; starting from the

estimated stresses in the simulation environment, it is possible to deduce the effects of vibrations on the user's well-being without the aid of instrumented vehicles [50–52].

The aim of our work was to quantify the regularity of the whole road surface on the basis of a MLS survey, as opposed to what is usually done with the standardized method (profilometer), for which the judgment of regularity is based only on the measurement of linear profiles.

The indices of regularity resulting from the application of the two methodologies on a stretch of road more than 3.5 km long were compared, as well as the judgments of regularity that resulted.

The chosen parameters for the creation of the digital model of the pavement were analyzed and justified. In addition, an estimate of the drive comfort was made on the generated surface and the judgement was compared with that deduced from the IRI and the geometric index.

2. Test Case

The test area consisted of a section of a secondary suburban road, about 4 km long, from km 10 + 350 to km 13 + 870.

It consisted of a single carriageway with two lanes, one in each driving direction, 3.60 m wide. It was located near a large industrial district, which was why there were different levels of irregularities produced by industrial vehicles on it. The analyses were carried out on the north carriageway (Figure 1).

Figure 1. (**a**) Overview of the test site. (**b**) A picture of the section of a secondary suburban road. (**c**) Mobile laser scanner (MLS) cloud density map.

The LiDAR survey was carried out with an MLS Riegl VMX-450 mounted on the roof of a car. The MLS system was equipped with inertial and global navigation satellite system (GNSS) sensors, housed under an aerodynamic protection dome, in order to be able to perform moving scans and to georeference them in an external reference system (ETRF00). The system consists of two Riegl VQ-450 laser scanners inclined by 35°, each with a 360° field of view (type of configuration called "Butterfly"). Table 1 provides some details about the data acquisition and the point cloud obtained.

Table 1. Main MLS data parameters.

Frequency	550 kHz (1.1×10^6 points/s)
MLS velocity	55 km/h
Density	4000 points/m^2
Line scan distance	7 cm
Number of points	150×10^6

For comparing the roughness indices computed on the surface modelled using MLS data with the standardized index, we carried out a regularity measurement with a high-speed inertial profilometer. The profilometer bar, installed on the front of the instrumented

vehicle, consisted of two lasers about 2 m apart; the elevation values were acquired at longitudinal intervals of 100 mm, and the set frequency was 62.5 kHz.

The profilometer was equipped with a GNSS positioning system to measure its trajectory. The profilometer measurement was made for a stretch of road between km 10 + 350 and km 13 + 870. IRI values provided by the profilometer were given for 10 m long segments, which led to 352 values being obtained. Table 2 shows the main parameters of measurement made with profilometer.

Table 2. Main profilometer data parameters.

Velocity	55 km/h
N° laser	2
Frequency	62.5 kHz
Laser distance	2 m
Positioning	GNSS single frequency

3. Methods

The road surface roughness analysis method we developed was based on the computation of two main roughness indices:

- The International Roughness Index, computed using data by mobile laser scanner (IRI_{MLS}) and coming from the inertial profilometer (IRI_{PROF}).
- The standard deviation of longitudinal roughness (σ), computed using data by mobile laser scanner (σ_{MLS}).

Data processing was carried out in three main steps, as follows:

- The first step focused on the construction of a numerical model of the road surface built by interpolating the data acquired with mobile laser scanner. The built digital elevation model (DEM) was one especially designed for road pavements. Two different interpolation methods were implemented to estimate the elevation on the grid nodes in order to compare the results and choose the most efficient in terms of adherence to the surface and computational time.
- The second step consisted of computing the roughness indices (IRI_{MLS} and σ_{MLS}) on the built surface model and comparing them with the standardized index derived from the profilometer.
- The last step focused on the evaluation of the ride comfort.

Figure 2 shows a workflow of the procedure.

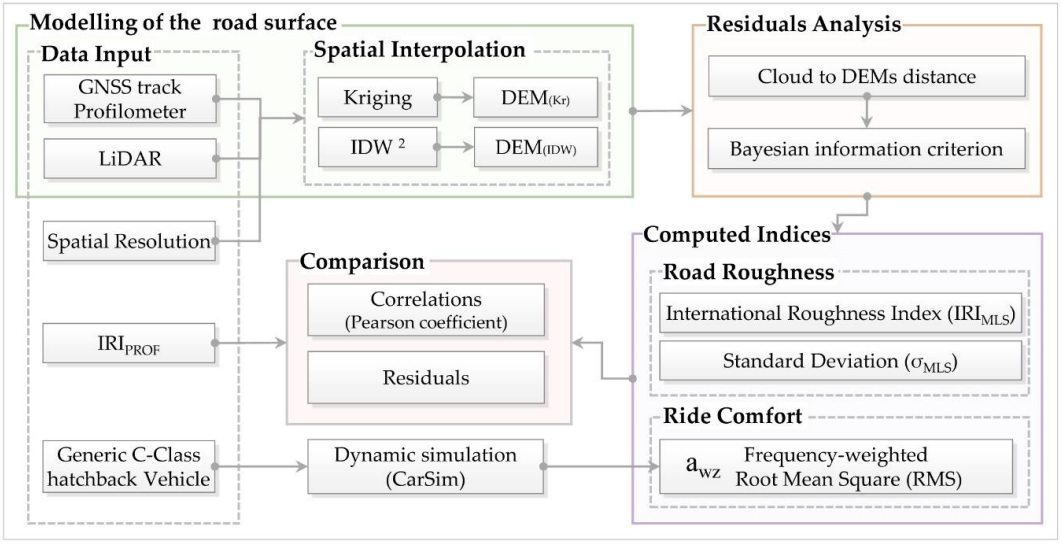

Figure 2. Workflow of data elaboration.

3.1. Modelling of the Road Surface

The pavement surface modelling required the interpolation of the MLS data on the nodes of a grid. Since the road planimetry usually includes straight and curved lines and also the vehicle equipped with the profilometer had in turn variations with respect to the layout, we believe that a grid DEM with a north–south direction was not suitable for building a reliable model.

To overcome this issue, we designed and implemented a specific algorithm able to generate a curvilinear abscissa grid, hereafter called DEMc [24]. The direction of the abscissa can follow the axis of the road or the GNSS track of the profilometer. The curvilinear grid was organized in a matrix at different levels, composed by n rows equal to the number of nodes constituting the generic longitudinal profile and by c columns equal to the number of nodes constituting the generic cross-section. To each node was assigned an elevation value derived from interpolation.

To choose the grid step to be set, we used the formula proposed by Hengl [53], which relates the data density to the resolution of the regular grid. The minimum resolution value ρ can be estimated with the following formula:

$$\rho = 0.5\sqrt{\frac{1}{D}} \tag{1}$$

where D is the average density of the point cloud (number of points/dm^2).

The elevation value to be attributed to the node was estimated using two different interpolators in order to evaluate the effect of the interpolation method on the regularity analysis: ordinary kriging (OK) and inverse distance weighted (IDW) [24]. The latter is a less rigorous method than kriging and consumes less CPU (central processing unit) time.

Kriging is a geo-statistical interpolation method that uses a variogram that depends on the spatial distribution of data rather than on actual values [54]. Ordinary kriging is the most widely used kriging method. IDW is a local deterministic interpolation technique that computes the value to be attributed to the node as a weighted average of the distance of the sample points in a given neighborhood [55]. It considers that the points closer to the node will have more influence and weights the sample points with the inverse of their distance from the node. In the IDW method, the main factor influencing the accuracy of the interpolator is the power value.

The best results are obtained using a power of 2 [56]. Powers greater than 4 produce slight differences in the resulting surface while increasing computational time, whereas a power equal to 1 produces a smoothed output [57]. Both interpolation methods were implemented in MATLAB to build the DEMc. The quality of the built DEMc was evaluated by estimating the "cloud to cloud distance", implemented in the open source software CloudCompare [58].

The default way to compute distances between two point clouds is the "nearest neighbor distance"—for each point of the compared cloud, CloudCompare searches the nearest point in the reference cloud and computes their (Euclidean) distance. When the nearest point in the reference cloud has been determined, the reference cloud (underlying) surface is locally modelled by fitting a mathematical model on the "nearest" point and several of its neighbors.

The distance from each point of the compared cloud to its nearest point in the reference cloud was replaced by the distance to this model. This was statistically more precise and less dependent on the cloud sampling. The local model used was a plan.

The criterion used is the Bayesian information criterion (BIC), a criterion for selecting the model from a finite set of models; the model with the lowest BIC was chosen. When adapting models, it is possible to increase the probability by adding parameters, but this can lead to over-adaptation. The BIC tries to solve this issue by introducing a penalty term for the number of parameters in the model. The whole process was implemented in MATLAB.

3.2. IRI Evaluation

In order to compute the IRI_{MLS}, we implemented an algorithm based on quarter-car simulation (QCS) [7] in MATLAB. The mathematics of IRI_{MLS} computation is

$$IRI_{MLS} = \frac{1}{L}\int_0^t \left|z_s' - z_u'\right| dt \quad (2)$$

where L is the length of the road section; t is the time of the simulation; and z_s' and z_u' are the vertical speeds of the sprung and un-sprung mass, respectively. IRI_{MLS} was computed on each longitudinal profile of the road surface.

The σ_{MLS} formula is as follows:

$$\sigma_{MLS} = \sqrt{\frac{\left[n\sum d_i^2 - \left(\sum d_i\right)^2\right]}{n(n-1)}} \quad (3)$$

where d_i is the deviation of the ith elevation from a simple linear regression for an assigned base-length (3.5 m), and n is the number of elevation values in the base-length [13].

When implementing the algorithm, the weight of the σ depends on the length of the fixed interval (mm/m). Both indices were computed on any profile extracted from the DEMc of the road surface measured with MLS, having a curvilinear abscissa corresponding to the GNSS track of the profilometer. These indices were compared with the values derived from standardized profilometer measurements.

In order to take the uncertainty of the GNSS positioning system mounted on the profilometer into account, we implemented an algorithm that identifies the values numerically closest to the reference values (profilometer) in correspondence with the same milestone.

Such values are considered to be those with the lowest residue, computed as the absolute value of the differences between IRI_{PROF} and IRI_{MLS}. At the same time, the planimetric deviation in transverse direction between the track composed by these "minimum distance" points and the theoretical track given by the laser profiles on the interpolated surface is computed in order to verify if the deviation between the two tracks is in accordance with the accuracy of GNSS.

The uncertainty on the IRI computation is also related to the sampling step of the longitudinal profile; the maximum error peak is around 167 mm, the maximum allowable sampling interval is around 300 mm [59]. Between two consecutive points, the profile trend can be schematized as a linear function, a quadratic function, or a zero slope function (horizontal line). For intervals less than or equal to 50 mm, the difference between local models is not significant, it is significant for larger intervals [7]. A few studies show that the function that best approximates the trend is the linear function (the straight line connecting the points of the profile), as long as the inter-distance between the points does not exceed 300 mm for accurate measurements and 600 mm for less accurate measurements [7].

Chin [27] suggested an optimal sampling step for MLS data by demonstrating that a sampling range between 100 and 300 mm provides IRI values comparable (with a tolerance of ±5%) with those derived from standardized high-precision techniques (rod and level) and inertial profilometer. Following their indications, we used a linear model between two profile points and a spacing in accordance with the data density.

The analysis was carried out by computing the roughness values according to two different methods: IRI_{MLS} and σ_{MLS} on the DEMc surface, distinguishing the values of the right track from those of the left track. Each of these groups of values was compared with the recorded values on the corresponding traces.

The values of IRI_{MLS} and σ_{MLS} were computed over 10 m intervals in order to make a reliable comparison with the corresponding values derived by the profilometer (IRI_{PROF}). Since the road surface measured was more affected on the right side than on the left side, it was advisable for us to choose a small sampling interval in the IRI calculation (10 m) in order to highlight the localized effects. In particular, the sections were analyzed separately, dividing into two groups according to the value of the IRI (ASTM-E1926 [60])—the first

group for IRI < 3.5 m/km and the second group for IRI > 3.5 m/km. The regularity computed for these sub-segments was compared with the regularity conditions of the corresponding segments on the DEMc, measured with the dynamic and geometric method.

3.3. IRI Evaluation of Ride Comfort

An assessment of the effects of vibrations on human comfort can be made by analyzing the vertical acceleration; in particular, according to the ISO 2631-1 [61], the frequency-weighted root mean square (RMS) accelerations (a_{wz}) is

$$a_{wz} = \sqrt{\sum \left(w_{k,i} \cdot a_{iz}^{RMS}\right)^2} \quad (4)$$

where $w_{k,i}$ is the value of the weight factor, and a_{iz}^{RMS} is the value of the RMS acceleration, computed using the power spectral density.

The vertical accelerations were computed using the dynamic simulation software package CarSim@ by Mechanical Simulation Corporation on the DEMc of the road surface.

Finally, the evaluation of comfort levels was assessed according to the values shown in Table 3.

Table 3. Comfort levels related to a_{wz} threshold values proposed by ISO 2631-1.

a_{wz}	Comfort Level
Less than 0.315 m/s^2	Not uncomfortable
0.315–0.63 m/s^2	A little uncomfortable
0.5–1.0 m/s^2	Fairly uncomfortable
0.8–1.6 m/s^2	Uncomfortable
1.25–2.5 m/s^2	Very uncomfortable
Greater than 2 m/s^2	Extremely uncomfortable

4. Results and Discussions

4.1. Modelling the Road Surface

In order to build the DEMc using the kriging interpolation algorithm, we estimated the experimental semi-variogram; the lag was chosen so as not to have loss of detail and excessive smoothing of the variogram. A Gaussian' variogram model with nugget and absence of anisotropy was adapted to the experimental variogram model (Figure 3).

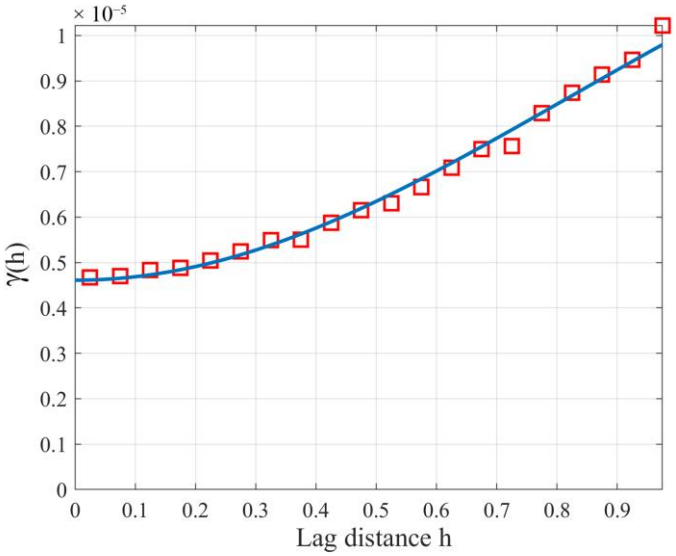

Figure 3. Experimental variogram and "Gaussian" variogram model.

The grid step of the DEMc was set at 100 mm, on the basis of the density of the point clouds, and equally spaced with the data acquired by the profilometer. The residuals were computed as the distance between the local plane fitting the point cloud and the built DEMs (with kriging and IDW); the local plane model was interpolated using a number of points equal to the default number (6 points).

We used the BIC method (see Section 3.1) to find the probability distribution functions that best fit the residuals. For the DEM interpolated with ordinary kriging, the function that best interpolated the residuals was Weibull, while for IDW, it was the beta distribution (Figure 4).

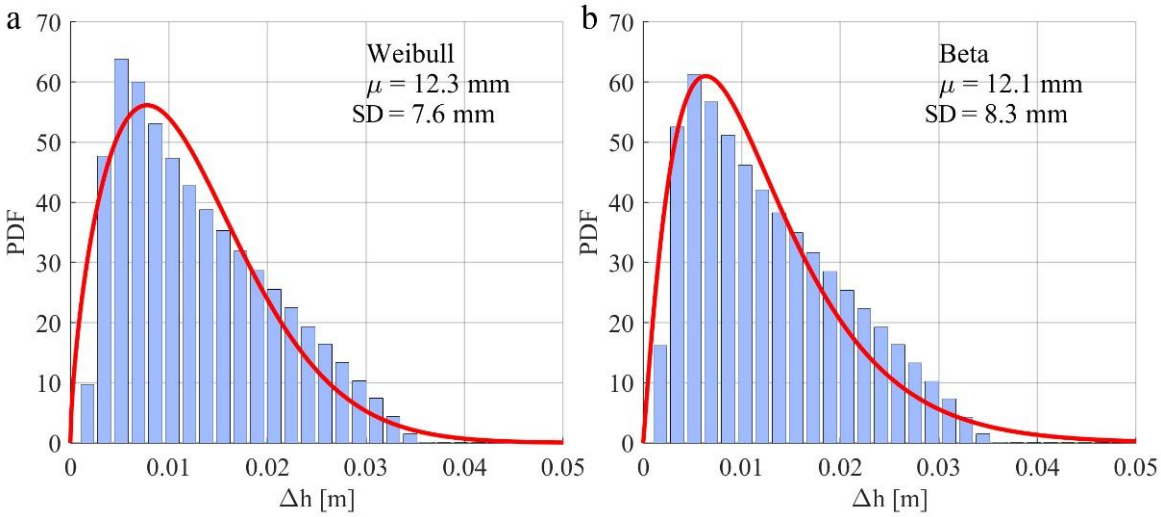

Figure 4. Probability distribution functions that best fit the residues. (**a**) Ordinary kriging; (**b**) inverse distance weighted IDW^2.

Looking at the statistical results, it is possible to observe how the surfaces generated with ordinary kriging were similar to those generated with IDW. The processing times were very different, around 30 min for IDW and 10 h for kriging. Data processing was carried out with a Dell precision tower 3620 workstation, 32 Gb Ram, 500 Gb SSD storage; an Intel Xeon E3 1200 V5 processor; and a Radeon Pro WX5100 GPU. The choice of the interpolator to be used was related to the more or less homogeneous distribution of the data and was a function of the characteristics that are to be highlighted. The data distribution was therefore a key element in the choice of the interpolation method, regardless of its robustness. Tan and Xu [62], following tests on a set of experimental data, deduced that, to model homogeneously distributed data like our own, IDW and kriging give results, in terms of root mean square error and mean absolute error, of the same order of magnitude. In this work, we chose to use kriging, even if its computational cost is higher, as it is recognized in the literature as a more robust interpolator.

4.2. IRI Evaluation

The regularity analysis was carried out by computing the IRI values on a number of segments 10 m long; over the total length analyzed (3520 m), 352 values were obtained for each wheel track.

For each segment, the IRI_{MLS} and σ_{MLS} values on the DEMc were computed and compared with the corresponding IRI values derived from the inertial profilometer (IRI_{PROF}). The results for right and left tracks were analyzed separately. The boxplot of IRI differences ($IRI_{PROF} - IRI_{LSM}$ and $IRI_{PROF} - \sigma_{LSM}$) and the associated standard deviations (SD) are shown in the box in Figure 5.

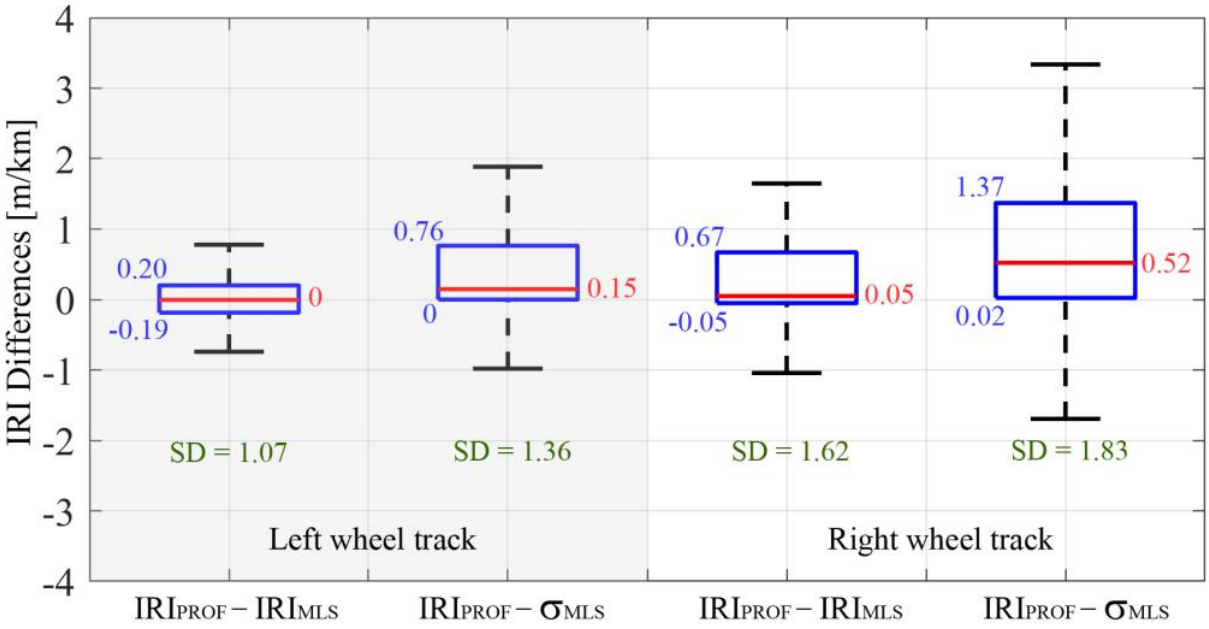

Figure 5. Box plots of the International Roughness Index (IRI) differences.

For all cases, the standard deviation of the residuals was lower than 2 m/km. The comparison of the values showed a strong correlation between the values of IRI_{MLS} and IRI_{PROF}, characterized by Pearson coefficients of 0.82 (left track) and 0.70 (right track) (Figure 6).

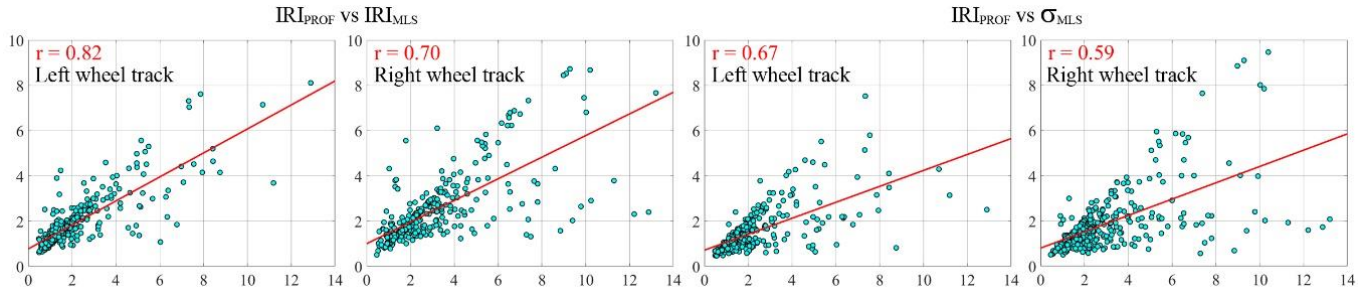

Figure 6. Diagrams of correlations.

The correlation between the σ_{MLS} and IRI_{PROF} was lower, given that the Pearson coefficients were 0.67 (left track) and 0.59 (right track) (Figure 6).

The diagrams in Figure 7 show the trend of the values computed on the left wheel track and the differences (in absolute value) between both IRI_{MLS} and σ_{MLS} with IRI_{PROF}. The red and blue dots at the top of the figures show the segments (10 m long) with IRI greater than 3.5 m/km. The black line in the IRI diagrams highlights the values within the regularity threshold.

The diagrams in Figure 8 show results for the right wheel track.

Observing the box plots (Figure 5), the correlation diagrams (Figure 6), and the IRI diagrams (Figures 7 and 8), one notices a large spread of the measured values, which highlights the occurrence of outliers in the dataset. Their occurrence may be due to

- The vehicle with the profilometer bar being subjected to transverse oscillations during the motion, since the operator was not able to fully maintain the intended trajectory; skidding in the direction transverse to the motion significantly afflicted the values, resulting from the measurement of the profiles, mainly when the road segment was highly distressed (right trace, Figure 8). In detail, the IRI computed on 10 m long sec-

tions was more affected by localized defects [20]; hence, the probability of highlighting one due to the skidding of the profilometric bar was quite high.

- The differences observed were probably due to the dynamic response of the profilometer. The acquisition speed was variable (from 30 to 60 km/h), and thus large variations in acceleration probably led to errors in the measurement of the profiles and therefore in the computation of IRI [16].
- The poor accuracy in trajectory measurement due to positioning errors of the profilometer's single-frequency GNSS receiver together with the imperfect knowledge of the offsets between trajectory and profilometer bar did not allow an accurate determination of laser profilometer traces [63].

Although we implemented an algorithm capable of accounting for transverse oscillation, the effects produced and highlighted in the second and third bullet points can certainly contribute to the generation of outliers, mainly concentrated in very distressed sections.

Observing the red and blue dots (Figures 7 and 8), one can notice how these tend to form homologous clusters only in correspondence of sections with adjacent dots (contiguous and greater than 10 m).

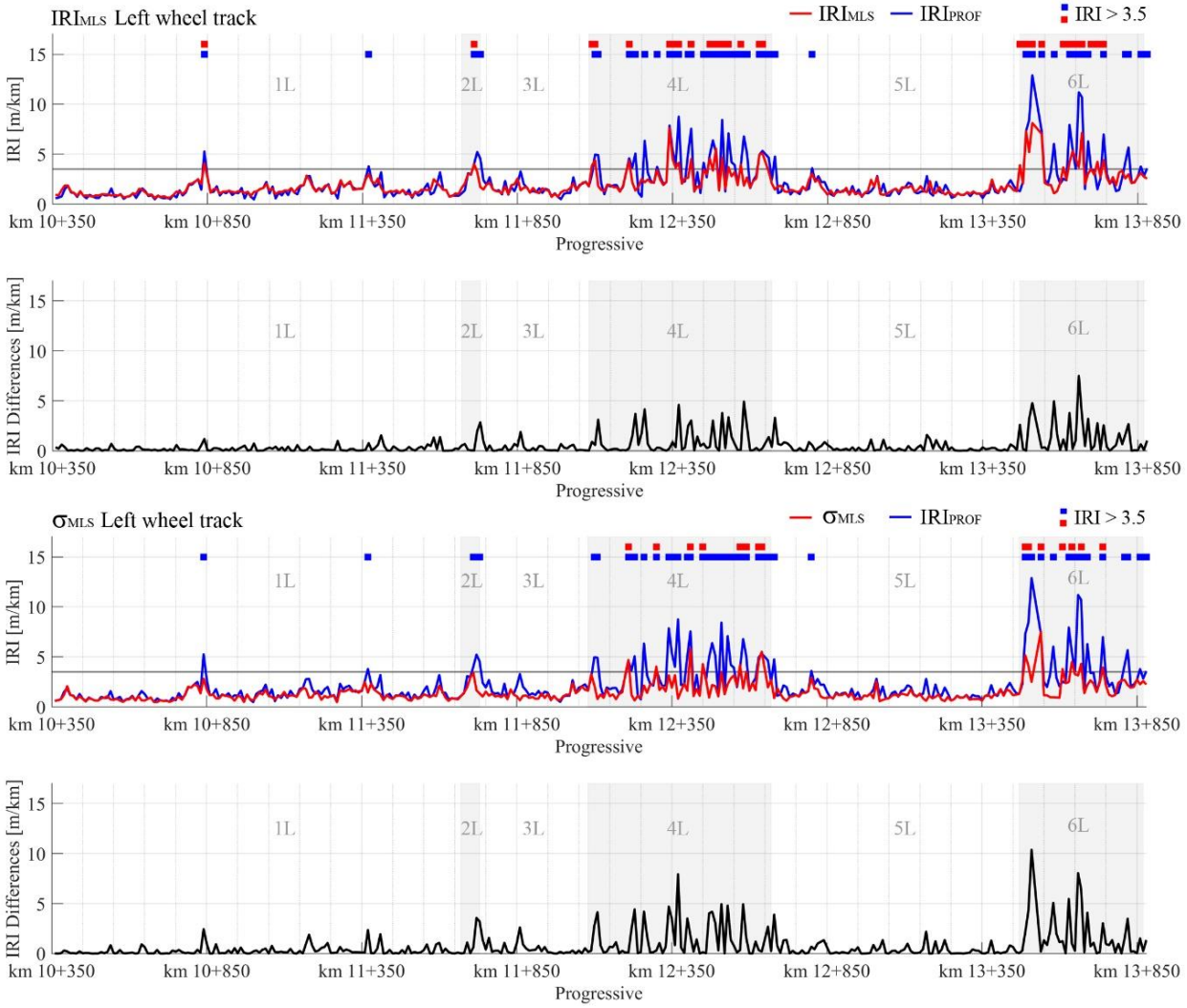

Figure 7. Left wheel track. Comparison between roughness indices: International Roughness Index computed using data by mobile laser scanner (IRI_{MLS}) and standard deviation of longitudinal roughness (σ) computed using data by mobile laser scanner (σ_{MLS}) vs. inertial profilometer (IRI_{PROF}).

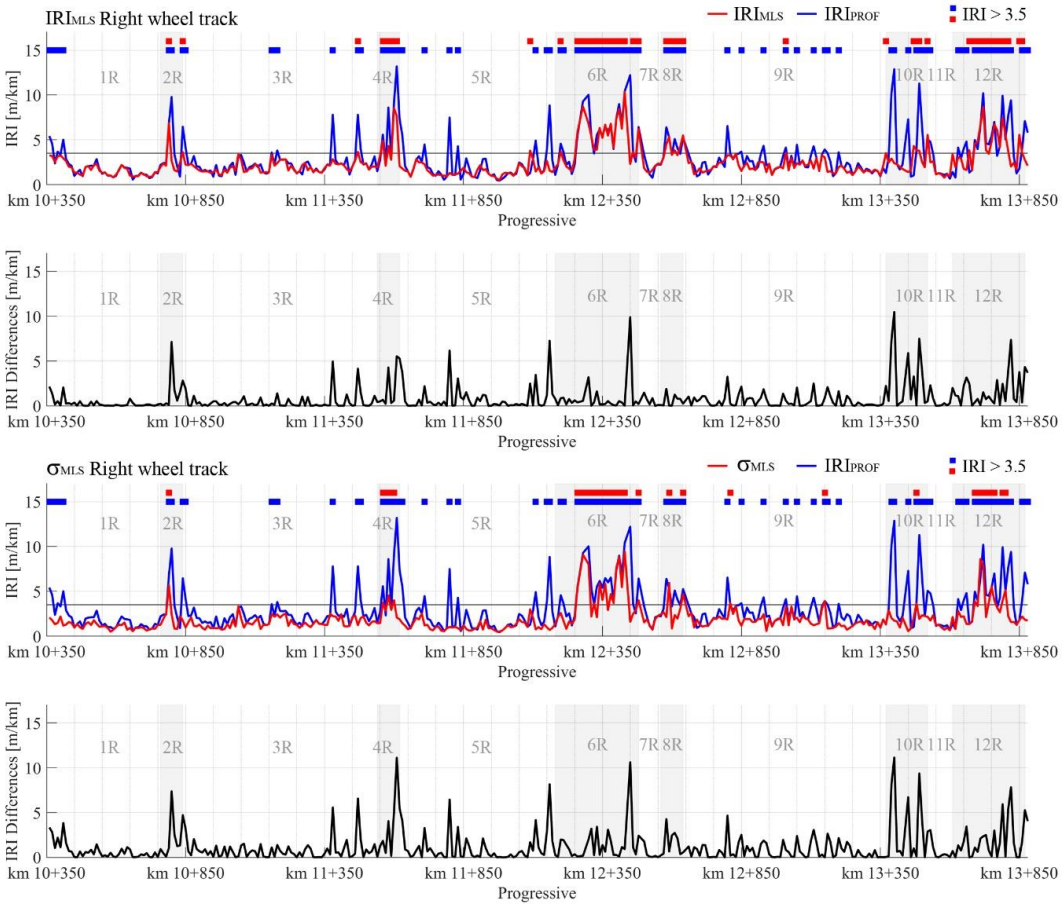

Figure 8. Right wheel track. Comparison between roughness indices: IRI_{MLS} and σ_{MLS} vs. IRI_{PROF}.

The analysis of these clusters was used to subdivide the entire section in more sub-sections, in particular:

- Sub-sections with grouped dots (grey background, 2L, 4L, and 6L for the left track and 2R, 4R, 6R, 8R, 10R, and 12R for the right track); these sub-sections identified sections with repetitive irregularities, not localized;
- Sub-sections with isolated dots (1L, 3L, and 5L for the left track and 1R, 3R, 5R, 7R, 9R, and 11R for the right track); isolated dots represent sections that are probably characterized by the presence of localized distress (isolated defects) and therefore not very significant for network analysis.

Eighteen sub-sections with a length ranging between 60 and 1320 m were identified, 6 for the left wheel track and 12 for the right one. Among all 18, 9 were classified as having a good regularity with an average IRI_{PROF} value of 1.79 m/km and 9 sections were classified as having low regularity with an average IRI value of 4.56 m/km (Tables 4 and 5, showing the profilometer values).

Table 4. Segment characterization (left wheel track).

Segment	Length (m)	Mean IRI_{PROF}	SD
1L	1320	1.33	0.70
2L	60	3.71	1.07
3L	350	1.60	0.65
4L	590	3.64	2.04
5L	800	1.45	0.57
6L	400	4.32	2.93

Table 5. Segment characterization (right wheel track).

Segment	Length (m)	Mean IRI_{PROF}	SD
1R	410	1.91	1.13
2R	80	4.49	2.96
3R	700	2.26	1.18
4R	80	6.85	3.52
5R	560	1.97	1.58
6R	300	5.61	2.78
7R	80	2.13	0.86
8R	80	4.54	1.13
9R	730	2.41	1.03
10R	150	5.16	3.96
11R	90	1.36	0.81
12R	260	4.95	2.04

The IRI values shown in Figures 7 and 8 were computed on 10 m segments; the higher differences occurred in correspondence with very damaged surfaces, i.e., where isolated defects were also recorded.

The roughness value on each homogeneous section of the development between 60 and 1320 m was computed as an average of the values recorded on the relative 10 m segments; in this case, the differences of IRIs in the different methods were decreased, exceeding 2 m/km only on two sections, i.e., on a total length of 230 m, equal to 6.5% of the total development.

For each of these sections, the average IRI_{MLS} and σ_{MLS} values were computed and compared with the corresponding profilometer values (Table 6). In most cases, the IRI_{MLS} and σ_{MLS} values were lower than the profilometric values (IRI_{PROF}), and this sometimes led to a change in class. This happened for a total section length of 1280 m (18.2% of total length) for the dynamic index and 1700 m (24.1% of total length) for the σ_{MLS}.

Table 6. Variation of IRI values along the 18 identified homogeneous segments.

Segment	Length (m)	Mean IRI_{PROF}	Mean IRI_{MLS}	Δ (%)	Mean σ_{MLS}	Δ (%)
1L	1320	1.33	1.40	5	1.10	17
2L	60	3.71	2.74	26	2.06	44
3L	350	1.60	1.60	0	1.25	22
4L	590	3.64	2.78	24	2.16	41
5L	800	1.45	1.47	1	1.15	21
6L	400	4.32	3.39	22	2.50	42
1R	410	1.91	1.71	10	1.18	38
2R	80	4.49	2.88	36	2.15	52
3R	700	2.26	1.97	13	1.52	33
4R	80	6.85	4.27	38	2.93	57
5R	560	1.97	1.54	22	1.14	42
6R	300	5.61	4.93	12	4.12	27
7R	80	2.13	2.00	6	1.83	14
8R	80	4.54	4.05	11	2.90	36
9R	730	2.41	2.04	15	1.72	29
10R	150	5.16	2.77	46	1.85	64
11R	90	1.33	1.60	20	1.23	8
12R	260	4.95	4.05	18	3.07	38

It should be noted that the change of class mainly concerned the sections characterized by a few points above the threshold; especially in the case of the dynamic index, there was a significant reduction, greater than one unit, only for three sections (4.6% of the total length of the sample road). In the case of the geometric index, there was a more significant change in class for eight sections (16.1% of the total length of the road). It should be noted

that the most troublesome sub-sections (IRI_{PROF} > 3.5) were well identifiable also with the indices derived from laser scanner measurements; in most cases, they were the same identified with the standard method (IRI_{PROF}).

It should be noted that the results depended strongly on the development of each section analyzed—the major differences in regularity were found on the shorter sections with the most damaged surfaces (Figure 5). These differences were, in fact, mainly present for developments of less than 250m (Table 6), and this can be explained by the effect of overlapping between localized distress and regularity. This points to the need for a standardization of the development of the sections to be measured, in accordance with the results of the experimental studies conducted by Sayers et al. [6].

However, the analysis of the correlation of the regularity values computed with the two indices (IRI_{MLS} and σ_{MLS}) showed in these sections a very good correlation with the values obtained by the profilometer. Figure 9 shows the correlation diagrams together with the corresponding correlation and determination coefficients.

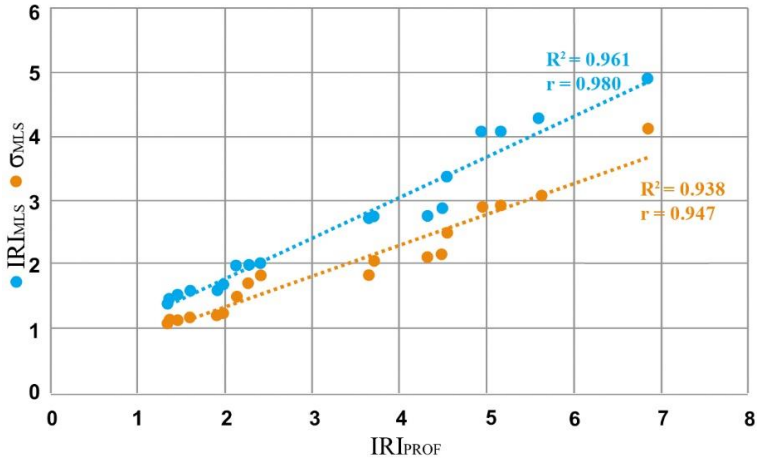

Figure 9. Correlation between IRI_{PROF}, IRI_{MLS}, and σ_{MLS}.

4.3. Evaluation of Ride Comfort

The evaluation of the ride comfort was carried out using the CarSim software package. To run the simulation, we used a Generic C-Class vehicle hatchback with Strut front and 5-Link rear suspension. C-Class vehicles include the following car models: Audi A3, Chevrolet Cruze, Ford Focus, and Opel Astra.

The DEM of the road surface was provided as input for the simulator in order to compute the weighted root mean square of the vertical accelerations acting on the vehicle. The computation of the accelerations was carried out at different speeds (40, 60, 80, and 100 km/h). The results are shown in the diagram (Figure 10).

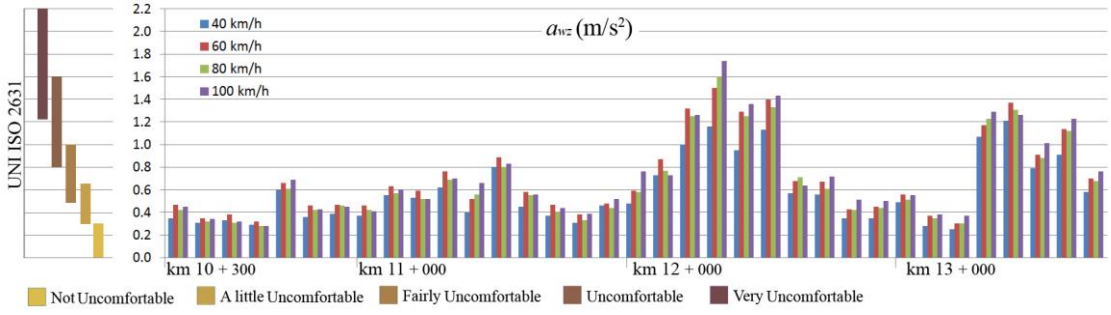

Figure 10. Vertical weighted root mean square (RMS) acceleration (a_{wz}).

It is possible to notice that there was a good correlation between the IRI_{PROF} values and the vertical accelerations, meaning with the ride comfort.

At segments characterized by an IRI value close to or greater than 3.5 m/km, the vertical acceleration was greater than 0.8 m/s^2, thus falling within the class defined as "uncomfortable". If a threshold value for the perception of discomfort equal to 0.4 m/s^2 [64] was set, the judgments were even more consistent with those derived from the IRI_{PROF} values. This further highlights the potential of the methodology we proposed.

The influence of driving speed generally does not change the comfort class according to UNI ISO 2631-1 [61], although at higher speeds, the influence on comfort is stronger if the road is more damaged [64].

A comparison of the vertical accelerations recorded at 40 km/h with those at 100 km/h shows that the average increase was 23.1%. The same average increase reached 40% along the most damaged segments.

5. Conclusions

The availability of new technologies is focusing researchers' attention back on geometric road surveys. In the recent past, the dynamic analysis of the response of an instrumented vehicle has represented a technological alternative to overcome the drawbacks of geometric surveys (low productivity, high impact on traffic flow, etc.). The aim of our study was to compare regularity measurements derived by standardized techniques, namely, by profilometer, with those by MLS.

On the basis of the experimental tests we performed and the results we obtained, we can conclude that

- The DEM with a curvilinear abscissa that was specifically designed and implemented for the road pavements allows us to model road sections several tens of kilometers long in order to run on the entire surface regularity analysis, without limitations due to the computational power, an issue experienced on grid models with north–south direction.
- The comparison between the indices derived by the profilometer and those computed on the DEM produced positive results; the correlations were good and proved the potential to quantify the regularity of the whole surface against the measurement on linear profiles only, but were unsuitable in terms of representing the surface in its real complexity.
- The differences between the IRI values derived from profilometer and the values derived from DEM were small enough not to change and substantially affect the evaluation of the single sections, which is useful for planning maintenance works.
- The critical sub-sections identified using the standardized method (profilometer) coincided, except for those where localized defects were present, with the critical sub-sections identified by the indices derived from MLS measurements. This meant that the method could be used for a quick analysis at the network level.
- The values obtained, in terms of comfort, were in line and were strongly correlated with those deduced from standard methodology. This showed a double use of the implemented DEM; in addition to being used for an estimation of the regularity extended to the entire paved surface, it also allowed for the estimation of driving comfort through dynamic simulation.

The authors are confident that the progress of their studies can lead to the development of a strong tool for a good and deep knowledge of a wide road network, thus helping to evaluate and plan maintenance work.

Author Contributions: Conceptualization, M.R.D.B., A.D.B., M.F., and M.G.; data supply, M.G.; methodology, M.R.D.B., A.D.B., and M.F.; software, A.D.B.; validation, M.R.D.B. and M.F.; formal analysis, M.R.D.B., A.D.B., and M.F.; writing—original draft preparation, M.R.D.B., A.D.B., and M.F.; writing—review and editing, A.D.B. All authors have read and agreed to the published version of the manuscript.

Funding: This research received no external funding.

Data Availability Statement: The data presented in this study are available on request from the corresponding author.

Conflicts of Interest: The authors declare no conflict of interest.

References

1. Szénási, S.; Kertész, G.; Felde, I.; Nádai, L. Statistical accident analysis supporting the control of autonomous vehicles. *J. Comput. Methods Sci. Eng.* **2020**, 1–13. [CrossRef]
2. Tighe, S.; Li, N.; Cowe Falls, L.; Haas, R. Incorporating road safety into pavement management. *Transp. Res. Rec. J. Transp. Res. Board* **2000**, *1699*, 1–10. [CrossRef]
3. ISO. *Characterization of Pavement Texture by use of Surface Profiles—Part 2: Terminology and Basic Requirements Related to Pavement Texture Profile Analysis*; ISO 13473-2; International Organization for Standardization: Geneva, Switzerland, 2002.
4. ISO. *Characterization of Pavement Texture by Use of Surface Profiles—Part 3: Specification and Classification of Profilometers*; ISO 13473-3; International Organization for Standardization: Geneva, Switzerland, 2002.
5. ASTM. *Standard Terminology Relating to Vehicle-Pavement Systems*; E867-06; ASTM International: West Conshohocken, PA, USA, 2020.
6. Gillespie, T.D.P.; Queiroz, C.A.V.; Sayers, M.W. *The Internationa Road Roughness Experiment: Establishing Correlation and a Calibration Standard for Measurements*; World Bank: Washington, DC, USA, 1986.
7. Sayers, M.W. On the calculation of international roughness index from longitudinal road profile. *Transp. Res. Rec.* 1995.
8. Gillespie, T.D.; Sayers, M.W.; Segal, L. *Calibration of Response-Type Road Roughness Measuring Systems: NCHRP Rep. 228*; Transportation Research Board: Washington, DC, USA, 1980.
9. Perera, R.W.; Kohn, S.D.; Wiser, L.J. Factors contributing to differences between profiler and the international roughness index. *Transp. Res. Rec.* **2006**, *1974*, 80–88. [CrossRef]
10. UNI EN. *Road and Airfield Surface Characteristics—Test Methods—Part 5: Determination of Longitudinal Unevenness Indices*; EN 13036-5; European Committee for Standardization: Brussels, Belgium, 2019.
11. ASTM. *Standard Test Method for Measuring Road Roughness by Static Level Method*; E1364-95; ASTM International: West Conshohocken, PA, USA, 2017.
12. UNI EN. *Road and Airfield Surface Characteristics—Test Methods—Part 7: Irregularity Measurement of Pavement Course: The Straightedge Test*; EN 13036-7; European Committee for Standardization: Brussels, Belgium, 2019.
13. Muniz de Farias, M.; de Souza, R.O. Correlations and analyses of longitudinal roughness indices. *Road Mater. Pavement Des.* **2009**, *10*, 399–415. [CrossRef]
14. Mubaraki, M.; Sallam, H. The most effective index for pavement management of urban major roads at a network level. *Arab. J. Sci. Eng.* **2020**. [CrossRef]
15. Múčka, P. Relationship between international roughness index and straightedge index. *J. Transp. Eng.* **2012**, *138*, 1099–1112. [CrossRef]
16. Lee, M.H.; Chou, C.P. Laboratory method for inertial profiler verification. *J. Chin. Inst. Eng.* **2010**, *33*, 617–627. [CrossRef]
17. Loizos, A.; Plati, C. An alternative approach to pavement roughness evaluation. *Int. J. Pavement Eng.* **2008**, *9*, 69–78. [CrossRef]
18. McGhee, K.K. *Quality Assurance of Road Roughness Measurement*; Virginia Transportation Research Council: Charlottesville, VA, USA, 2000.
19. ASTM. *Standard Test Method for Measuring the Longitudinal Profile of Traveled Surfaces with an Accelerometer-Established Inertial Profiling Reference*; E950/E950M-09; ASTM International: West Conshohocken, PA, USA, 2018.
20. Múčka, P. International roughness index specifications around the world. *Road Mater. Pavement Des.* **2017**, *18*, 929–965. [CrossRef]
21. Sayers, W.M.; Karamihas, S.M. *The Little Book of Profiling: Basic Information about Measuring and Interpreting Road Profiles*; University of Michigan Transportation Research Institute: Ann Arbor, MI, USA, 1998.
22. Barbarella, M.; De Blasiis, M.R.; Fiani, M. Terrestrial laser scanner for the analysis of airport pavement geometry. *Int. J. Pavement Eng.* **2017**, *20*, 466–480. [CrossRef]
23. Barbarella, M.; D'Amico, F.; De Blasiis, M.; Di Benedetto, A.; Fiani, M. Use of terrestrial laser scanner for rigid airport pavement management. *Sensors* **2018**, *18*, 44. [CrossRef] [PubMed]
24. De Blasiis, M.R.; Di Benedetto, A.; Fiani, M.; Garozzo, M. In Assessing the Effect of Pavement Distresses by Means of Lidar Technology. In Proceedings of the ASCE International Conference on Computing in Civil Engineering 2019American Society of Civil Engineers, Atlanta, Georgia, 17–19 June 2019.
25. De Blasiis, M.R.; Di Benedetto, A.; Fiani, M. Mobile laser scanning data for the evaluation of pavement surface distress. *Remote Sens.* **2020**, *12*, 942. [CrossRef]

26. Křemen, T.; Štroner, M.; Třasák, P. Determination of pavement elevations by the 3d scanning system and its verification. *Geoinform. FCE CTU* **2014**, *12*, 55–60. [CrossRef]
27. Chin, A. Paving the Way for Terrestrial Laser Scanning Assessment of Road Quality. Master's Thesis, Oregon State University, Corvallis, OR, USA, 2012.
28. Alhasan, A.; White, D.J.; De Brabanter, K. Spatial pavement roughness from stationary laser scanning. *Int. J. Pavement Eng.* **2017**, *18*, 83–96. [CrossRef]
29. De Blasiis, M.R.; Di Benedetto, A.; Fiani, M.; Garozzo, M. Characterization of Road Surface by Means of Laser Scanner Technologies, Pavement and Asset Management. In Proceedings of the World Conference on Pavement and Asset Management (WCPAM 2017), Baveno, Italy, 12–16 June 2017; CRC Press: London, UK, 2019; p. 63. [CrossRef]
30. Chang, J.; Chang, K.; Chen, D. Application of 3d laser scanning on measuring pavement roughness. *J. Test. Eval.* **2006**, *34*. [CrossRef]
31. Guan, H.; Li, J.; Cao, S.; Yu, Y. Use of mobile lidar in road information inventory: A review. *Int. J. Image Data Fusion* **2016**, *7*, 219–242. [CrossRef]
32. Conforti, D.; Zampa, F. Lynx mobile mapper for surveying city centers and highways. *Int. Arch. Photogramm. Remote Sens. Spat. Inf. Sci.* **2011**, *38*, 2011. [CrossRef]
33. Glennie, C. Kinematic terrestrial light-detection and ranging system for scanning. *Transp. Res. Record J. Transp. Res. Board* **2009**, *2105*, 135–141. [CrossRef]
34. Olsen, M.J.; Knodler, M.A.; Squellati, A.; Tuss, H.; Williams, K.; Hurwitz, D.; Reedy, M.; Persi, F.; Glennie, C.; Roe, G.V.; et al. *Guidelines for the Use of Mobile Lidar in Transportation Applications*; TRB NCHRP Final Report 748; TRB: Washington, DC, USA, 2013; p. 250.
35. Yen, K.S.; Ravani, B.; Lasky, T.A. *Lidar for Data Efficiency*; AHMCT Research Center: Davis, CA, USA, 2011.
36. Mendenhall, S. *Mobile Laser Scanning—Caltrans Evaluates the Technology's Costs and Benefits*; CE News; ZweigWhite: Fayetteville, AR, USA, 2011; pp. 42–43.
37. Williams, K.; Olsen, M.V.; Roe, G.; Glennie, C. Synthesis of Transportation Applications of Mobile Lidar. *Remote Sens.* **2013**, *5*, 4652–4692. [CrossRef]
38. Alhasan, A.; Younkin, K.; White, D. *Comparison of Roadway Roughness Derived from Lidar and Sfm 3d Point Clouds*; Trans Project Report; Iowa State University: Ames, IA, USA, 2015.
39. Alhasan, A. Quantifying Road Roughness: Multiresolution and Near Real-Time Analysis. Ph.D. Thesis, Iowa State University, Ames, IA, USA, 2015.
40. Kumar, P.; Lewis, P.; Mc Elhinney, C.; Rahman, A. An algorithm for automated estimation of road roughness from mobile laser scanning data. *Photogramm. Rec.* **2015**, *30*, 30–45. [CrossRef]
41. Kumar, P.; Angelats, E. An automated road roughness detection from mobile laser scanning data. *Int. Arch. Photogramm. Remote Sens. Spatial Inf. Sci.* **2017**, *XLII-1/W1*, 91–96. [CrossRef]
42. Tran, T.H.; Taweep, C. Automated extraction of expressway road surface from mobile laser scanning data. *J. Cent. S. Univ.* **2020**, *27*, 1917–1938. [CrossRef]
43. Fernando, E.G.; Walker, R.S. *Impact of Changes in Profile Measurement Technology on QA Testing of Pavement Smoothness: Project Summary*; A & M Transportation Institute: Bryan, TX, USA, 2013.
44. Fernando, E.G.; Walker, R.S.; Mikhail, M. Comparative testing of lasers for ride quality measurement on hot-mix asphalt pavements. *Transp. Res. Rec.* **2014**, *2457*, 19–29. [CrossRef]
45. Liu, C.; Herman, R. Road profiles, vehicle dynamics, and human judgment of serviceability of roads: Spectral frequency domain analysis. *J. Transp. Eng.* **1998**, *124*, 106–111. [CrossRef]
46. Liu, C.; Herman, R. Road profile, vehicle dynamics, and ride quality rating. *J. Transp. Eng.* **1999**, *125*, 123–128. [CrossRef]
47. Fuentes, L.; Camargo, R.; Martínez-Arguelles, G.; Komba, J.J.; Naik, B.; Walubita, L.F. Pavement serviceability evaluation using whole body vibration techniques: A case study for urban roads. *Int. J. Pavement Eng.* **2019**, 1–12. [CrossRef]
48. Zhang, J.; Wang, L.; Jing, P.; Wu, Y.; Li, H. Iri threshold values based on riding comfort. *J. Transp. Eng. Part B Pavements* **2020**, *146*, 04020001. [CrossRef]
49. Varunjikar, T.; Vemulapalli, P.; Brennan, S. Multi-Body Vehicle Dynamics Simulation based on Measured 3d Terrain Data. In Proceedings of the 3rd International Conference on Road Safety and Simulation, Indianapolis, IN, USA, 14–16 September 2011; Transportation Research Board: Washington, DC, USA, 2012.
50. Uys, P.E.; Els, P.S.; Thoresson, M. Suspension settings for optimal ride comfort of off-road vehicles travelling on roads with different roughness and speeds. *J. Terramech.* **2007**, *44*, 163–175. [CrossRef]
51. Eralta, A.O.; de Oliveira, A.N.; Campos, C.G.; Neto, R.T.C.; Caldeira, A.B. *Ride Comfort Analysis of an Awd Vehicle Travelling on Different Types of Pavements*; SAE Technical Paper 2017-36-0384; SAE: Warrendale, PA, USA, 2017. [CrossRef]
52. Chandramohan, N.K.; Gunasekar, R.; Sethubalan, B.; Kumar, V.; Dineshkumar, V. *Measurement of Vibration in Different Parts of the Two Wheeler and its Harmfulness to Human Body*; International Journal of Mechanical and Production Engineering Research and Development (IJMPERD) Volume: ISSN(P): 2249-6890; ISSN(E): 2249-8001 Special Issue 7; TJPRC Pvt. Ltd.: Tamil Nadu, India, 2018; Volume 8, pp. 493–501.
53. Hengl, T. Finding the right pixel size. *Comput. Geosci.* **2006**, *32*, 1283–1298. [CrossRef]

54. Wackernagel, H. Variogram cloud. In *Multivariate Geostatistics: An Introduction with Applications*; Wackernagel, H., Ed.; Springer: Berlin/Heidelberg, Germany, 2003; pp. 45–49.
55. Burrough, P.A.; McDonnell, R.; McDonnell, R.A.; Lloyd, C.D. *Principles of Geographical Information Systems*; Oxford University Press: Oxford, UK; New York, NY, USA, 2015.
56. Pham, T.; Huynh Van, C.; Tran, P.; Chau, T.; Đức, N. Impact of Power Value in Idw Interpolation Method on Accuracy of the Soil Organic Matter (Som) Mapping. In Proceedings of the International Conference on GeoInformatics for Spatial-Infrastructure Development in Earth & Allied Sciences (GIS-IDEAS), Hanoi, Vietnam, 4–6 December 2008; Hanoi University of Mining and Geology: Hanoi, Vietnam, 2009.
57. Asal, F.F. Investigating the effects of changing the idw power on the quality of the generated digital elevation models. *Int. J. Res. Stud. Sci. Eng. Technol* **2014**, *1*, 33–42.
58. GitHub Inc. CloudCompare 2.8.1 User Manual; Open Source Project. Available online: http://www.cloudcompare.org/doc/qCC/CloudCompare%20v2.6.1%20-%20User%20manual.pdf (accessed on 10 January 2020).
59. Karamihas, S.M.; Institute, U.o.M.T.R.; Administration, U.S.F.H. *Critical Profiler Accuracy Requirements*; University of Michigan, Transportation Research Institute: Ann Arbor, MI, USA, 2005.
60. ASTM. *Standard Practice for Computing International Roughness Index of Roads from Longitudinal Profile Measurements*; E1926-08; ASTM International: West Conshohocken, PA, USA, 2015.
61. ISO. *Mechanical Vibration and Shock—Evaluation of Human Exposure to Whole-Body Vibration—Part 1: General Requirements*; ISO 2631-1; International Standardization Organization: Geneva, Switzerland, 1997.
62. Tan, Q.; Xu, X. Comparative analysis of spatial interpolation methods: An experimental study. *Sens. Transducers* **2014**, *165*, 155.
63. de Bakker, P.F.; Tiberius, C.C.J.M. Real-time multi-gnss single-frequency precise point positioning. *GPS Solut.* **2017**, *21*, 1791–1803. [CrossRef]
64. Katu, U.; Desavale, R.; Kanai, R. Effect of Vehicle Vibration on Human Body—Rit Experience. In Proceedings of the 11th National Conference on Machines and Mechanisms, Indian Institute of Technology, New Delhi, India, 18–19 December 2003; pp. 1–9.